International Journal of Chemical Kinetics

WILEY

RESEARCH ARTICLE OPEN ACCESS

Experimental Kinetic Study of the Reactions of Hydroxyl Radicals With Three Oxymethylene Ethers and With 1,3,5-Trioxane, Tetrahydrofuran, and Tetrahydrofuran-d8

Miu G. Mach | Anne Wolf | Bianca Krumm | Felix Poschen | Christian Kühn | Matthias Olzmann

Institut für Physikalische Chemie, Karlsruher Institut für Technologie (KIT), Karlsruhe, Germany

Correspondence: Matthias Olzmann (matthias.olzmann@kit.edu)

Received: 13 March 2025 | **Revised:** 12 May 2025 | **Accepted:** 15 May 2025

Funding: Funded by the Deutsche Forschungsgemeinschaft (DFG, German Research Foundation)—Projektnummer 237267381—TRR 150.

Keywords: hydroxyl radicals | OME-*n* | oxymethylene ethers | tetrahydrofuran | trioxane

ABSTRACT

Polyoxymethylene dimethyl ethers, $CH_3O(CH_2O)_nCH_3$ with $n \geq 1$ (abbreviated in the literature also as OME-*n*, PODE*n*, POMDME*n*, or OMDME*n*) are currently discussed as renewable fuels. Despite fuel + OH reactions are crucial for the combustion chemistry and atmospheric degradation of fuels, experimental kinetic data on OME-*n* + OH do not exist in the literature for $n >$ 1; only estimated or theoretically calculated values are available. In the present work, we present an experimental kinetic study of the reactions OH + OME-2 and OH + OME-3. For verification and comparison, identical experiments were also performed on the somewhat better-known reactions of OH with OME-1 and with the cyclic ethers 1,3,5-trioxane (TRI, $C_3H_6O_3$) and tetrahydrofuran (THF, C_4H_8O) as well as its perdeuterated isotopologue (THF-d8, C_4D_8O). Rate coefficients were determined as a function of temperature and pressure in slow-flow reactors with the pulsed laser photolysis/laser-induced fluorescence technique. The experiments were performed at temperatures between 250 and 520 K and pressures ranging from 0.2 to 5 bar (OME-2), 0.2 to 10 bar (OME-3), 0.2 to 0.9 bar (OME-1, TRI), and 0.2 to 0.8 bar (THF, THF-d8) with helium as bath gas. No significant pressure dependence of the rate coefficients was observed. The generally very weak temperature dependences are parameterized in Arrhenius form. Structural influences on reactivity are discussed and compared with predictions from structure-reactivity relationships.

1 | Introduction

Polyoxymethylene dimethyl ethers, $CH_3O(CH_2O)_nCH_3$ with $n \geq 1$, are currently discussed as sustainable diesel substitutes [1, 2] and can be produced via renewable pathways [3, 4]. These compounds are also known as oxymethylene ethers (OMEs), and we will use the abbreviation OME-*n* throughout this work. However, we note that alternative abbreviations such as PODE*n*, POMDME*n*, or OMDME*n* are also common in the literature [3]. In the context of fuel applications, the reactions of OMEs with hydroxyl radicals are of particular importance due to their impact on both autoignition behavior and atmospheric degradation. Despite this role, experimental kinetic data on OH + OME-*n* reactions are not available in the literature for $n > 1$. Only for OH + OME-1, a number of experimental studies have been published so far [5–9]. Consequently, current kinetic models for the combustion of larger OMEs rely on calculated or estimated rate coefficients for these reactions [10–12].

In the present study, we report what is, to the best of our knowledge, the first experimental determination of the rate coefficients for the reactions of OH with OME-2 and OME-3. The temperatures in our study range from ca. 260 to 520 K at nominal pressures between 0.2 and 10 bar to cover tropospheric conditions

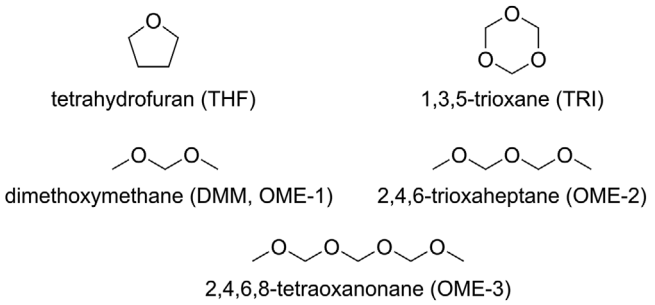

FIGURE 1 | Schematic structures of the compounds studied in this work.

and the beginning low-temperature ignition range. To validate our experimental approach, we reinvestigated the OH + OME-1 reaction and expanded the temperature and pressure ranges of earlier measurements [9].

To exemplify differences in the kinetics of open-chain and cyclic oligo ethers, the OH + 1,3,5-trioxane (TRI) reaction was also studied. TRI, which can be considered a cyclic analog of the open-chain OME-2, is also a potential feedstock in the industrial production of higher OMEs (see, e.g., [1, 3]). This raises the importance of understanding the kinetics of its atmospheric degradation to assess the overall environmental impact of OMEs as fuels. Few kinetic studies on the OH + TRI reaction are available in the literature [13–15]; their results will be discussed and compared with the findings of the present work.

Finally, to characterize differences between cyclic mono- and oligoethers, we studied the reaction of OH with tetrahydrofuran (THF) and its perdeuterated isotopologue (THF-d8). There are three earlier temperature-dependent studies of this reaction system, two at temperatures below 372 K (relative rate method [13, 16] and pulsed laser photolysis/laser-induced fluorescence [13]) and one above 800 K (shock tube [17]). In our study, we decrease the temperature gap in these measurements by performing experiments between ca. 300 and 500 K.

The structures of all oligoethers studied in the present work are shown in Figure 1. General aspects of the combustion chemistry of cyclic ethers were recently reviewed in Ref. [18].

2 | Experimental

The experiments were performed in three different slow-flow reactors (see below) by using the pulsed laser photolysis/laser-induced fluorescence (PLP/LIF) technique. The concentrations were chosen to ensure pseudo-first order conditions with respect to [OH]. The bath gas was helium. The general approach is well known and is described along with the experimental setups in detail elsewhere [9, 19–24]; only the essentials are repeated here.

The OH radicals were produced by pulsed photolysis of HNO_3 at 248 nm with a KrF excimer laser. The fluorescence of OH was excited with a frequency-doubled (BBO crystal) dye laser at 281.9 nm and detected with a photomultiplier non-resonantly around 308 nm. Two different LIF setups were employed. Setup A: Dye laser (dye: Coumarin 153) pumped by a XeCl excimer laser at 308 nm; detection of the fluorescence after passing a monochromator (308 ± 4 nm). Setup B: Dye laser (dye: Rhodamin 6G) pumped by a frequency-doubled Nd:YAG laser at 532 nm; detection of the fluorescence after passing a band pass filter (310 ± 10 nm). In both setups, digital delay generators were used to vary the time lag between the pulses of the photolysis laser and the fluorescence excitation laser. For each given delay time, ten measurements were recorded and automatically averaged. The repetition rate of the experiments was 10 Hz.

Three different reactors, corresponding to the temperature and pressure range of a specific experimental run, were used. The reactor for temperatures above 300 K and pressures above 1 bar (high temperature/high pressure, HTHP) is described in detail in Ref. [9], and the reactor for $T < 300$ K and $p < 1$ bar (low temperature/low pressure, LTLP) is described in Ref. [22]. The geometry of the third reactor, for $T > 300$ K and $p < 1$ bar (HTLP), very closely resembles that of the HTHP reactor [9]. All three reactors are made of stainless steel and have a T-shaped arrangement of three quartz windows. The laser beams for photolysis and fluorescence excitation propagate antiparallel through the two opposite windows, and the fluorescence is detected perpendicular to the laser axis through the third window. Due to the technical conditions within our laboratory, the HTHP reactor was always combined with Setup A and the HTLP and LTLP reactors were always combined with Setup B. We note that no systematic differences between the two setups were observed.

The gas mixtures (HNO_3/He and ether/He) were prepared manometrically in a separate mixing line and stored in two stainless steel cylinders at least for 12 h prior to use to ensure complete mixing. We note that this kind of mixture preparation ensures that the initial concentrations of the ethers are not influenced by their different vapor pressures. The flows (including neat He from a third cylinder) were regulated with mass-flow controllers and mixed in a capillary before entering the reactor. Flow rates were chosen so as to avoid accumulation of reaction products in the corresponding cell, and pseudo-first order conditions were carefully maintained. The ratios of the initial concentrations $[\text{ether}]_0/[\text{OH}]_0$ ranged between 25 and 5000, and all observed decays of the OH LIF signals were monoexponential. The absolute initial concentrations of the ethers ranged from 1×10^{14} to 3×10^{16} cm^{-3} and the initial concentrations of HNO_3 from 1×10^{15} to 6×10^{16} cm^{-3}. The latter range results in estimated OH initial concentrations between 7×10^{11} and 2×10^{13} cm^{-3} under the conditions of our experiments [9].

The OH radical precursor, HNO_3, was synthesized from freshly degassed concentrated H_2SO_4 and dried KNO_3 as described in Ref. [9]. The purities of the chemicals used were as follows: OME-1 ≥ 99.0% (Sigma–Aldrich), TRI ≥ 99.0% (Sigma–Aldrich), THF ≥ 99.8% (Carl Roth), THF-d8 ≥ 99.5%D (Carl Roth), He > 99.999% (Air Liquide), H_2SO_4 98% (Carl Roth), KNO_3 ≥ 99% (Carl Roth), OME-2 ≥ 99.7% and OME-3 ≥ 99.9% (Institute of Catalysis Research and Technology, KIT) [25].

3 | Results

We start this section with our investigations of OME-2 and OME-3, for which we present the first experimental kinetic data of

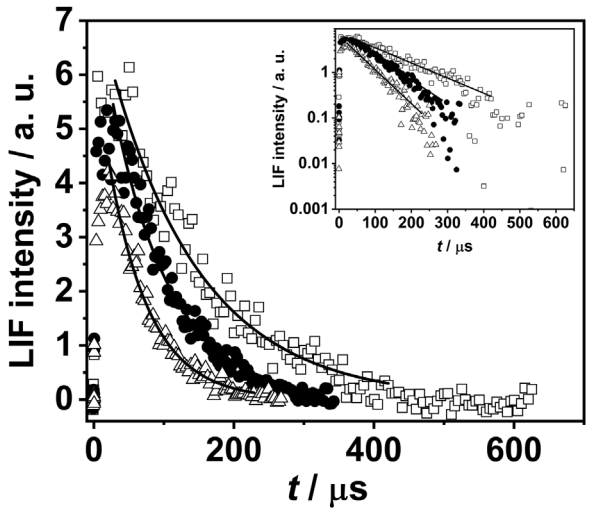

FIGURE 2 | Measured LIF intensity-time profiles (symbols) for the OME-2 + OH reaction and best mono-exponential fits (solid lines) for $T = 279$ K and $p = 900$ mbar at different OME-2 concentrations: (open squares) 2.55×10^{15}, (bullets) 5.08×10^{15}, and (open triangles) 7.60×10^{15} cm^{-3}.

their reactions with OH. We continue with OME-1, TRI, THF, and THF-d8, for which a limited number of studies have already been published. The data analysis for OME-2 + OH is elucidated in detail, whereas the presentations for the other reactions are kept shorter because the approaches were identical.

3.1 | The Reaction OME-2 + OH

The reaction OME-2 + OH → products was studied in the temperature range 261–514 K at pressures between 0.2 and 5 bar. Typical fluorescence intensity-time profiles of individual experiments are shown in Figure 2; pseudo-first order rate coefficients, k_{pseudo}, were obtained from mono-exponential fits. From these values, the second-order rate coefficients, k, were determined as the slopes of least-squares fits k_{pseudo} versus $[OME\text{-}2]_0$ as illustrated in Figure 3. Note that the finite intercepts at $[OME\text{-}2]_0 = 0$ are mainly due to unwanted side reactions of OH with impurities, most likely NO_2. This problem, which only marginally affects the slopes, is discussed at some length in Ref. [9]. The second-order rate coefficients, k, obtained in this way are tabulated along with the experimental conditions in Table S2. Because no significant pressure dependence was observed, we lumped and averaged these rate coefficients for the different pressures and temperatures close to each other ($T \pm \Delta T$) for further analysis. The results, $\langle k \rangle$, are collected in Table 1. The standard deviations $\sigma_{\langle k \rangle}$ given there were obtained as the sum of standard deviations of the mean plus the averaged standard deviations σ_k of the single k values from Table S2. The results are plotted in Figure 4.

As one can realize, there is notable scatter in the data for OME-2. It is somewhat larger than the scatter for the other compounds of the present work (see below) and larger than the typical scatter observed in previous studies performed with the same experimental setup (cf. Refs. [9, 23, 24, 26]). The reason is not quite clear. The experimental procedures were analogous, the compounds were of similar high purity, and there was no dependence observed on the age of the mixtures, on laser fluences, and on the direction of

TABLE 1 | Lumped and averaged (see text) rate coefficients of the OME-n + OH reactions.

R + OH	$(T \pm \Delta T)$/K	$(\langle k \rangle \pm \sigma_{\langle k \rangle})/10^{-12}$ cm^3/s
OME-1 + OH	253 ± 6	4.01 ± 0.68
	268 ± 5	4.11 ± 0.28
	272 ± 3	3.68 ± 0.82
	278 ± 3	3.85 ± 0.56
	282 ± 2	3.74 ± 0.37
	286 ± 1	3.63 ± 0.34
	294 ± 0	4.28 ± 0.50
	324 ± 2	3.90 ± 0.51
	357 ± 2	4.74 ± 0.21
	383 ± 1	4.18 ± 0.50
	420 ± 1	3.10 ± 0.24
	448 ± 1	3.22 ± 0.53
	503 ± 1	3.57 ± 0.19
OME-2 + OH	261 ± 6	5.60 ± 2.07
	265 ± 4	5.64 ± 2.20
	270 ± 4	3.68 ± 1.55
	278 ± 2	3.32 ± 0.88
	284 ± 2	7.32 ± 0.78
	288 ± 2	5.09 ± 1.55
	294 ± 1	5.74 ± 0.66
	310 ± 1	3.17 ± 1.08
	324 ± 2	4.75 ± 0.58
	341 ± 1	3.71 ± 0.92
	355 ± 2	6.19 ± 0.84
	359 ± 1	4.64 ± 1.13
	378 ± 1	4.69 ± 2.06
	384 ± 1	5.86 ± 0.74
	406 ± 1	4.41 ± 1.93
	424 ± 1	6.28 ± 0.79
	429 ± 1	3.21 ± 0.43
	455 ± 2	4.55 ± 0.48
	514 ± 2	5.63 ± 0.71
OME-3 + OH	284 ± 1	8.26 ± 1.17
	288 ± 1	6.67 ± 1.67
	295 ± 1	6.26 ± 1.01
	310 ± 1	7.29 ± 1.43
	319 ± 1	10.3 ± 2.14
	338 ± 1	7.01 ± 1.59
	356 ± 1	5.85 ± 1.06
	379 ± 1	5.42 ± 1.14
	410 ± 1	6.74 ± 1.78
	431 ± 1	7.83 ± 1.50
	456 ± 1	9.17 ± 1.87
	492 ± 1	8.66 ± 2.13
	519 ± 1	9.61 ± 2.21

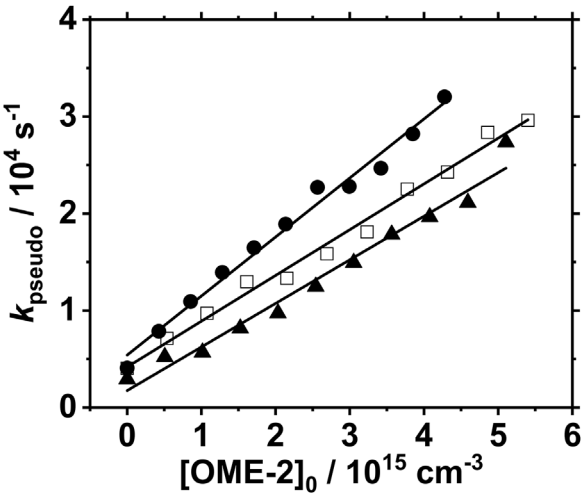

FIGURE 3 | Pseudo-first order plots at temperatures of (bullets) 405 K, (open squares) 322 K, and (triangles) 340 K at a nominal pressure of 2 bar. The best linear fits (solid lines) gave $k(405\ K, 2\ bar) = (6.09 \pm 0.23) \times 10^{-12}$ cm^3/s, $k(322\ K, 2\ bar) = (4.72 \pm 0.16) \times 10^{-12}$ cm^3/s, and $k(340\ K, 2\ bar) = (4.49 \pm 0.17) \times 10^{-12}$ cm^3/s, respectively.

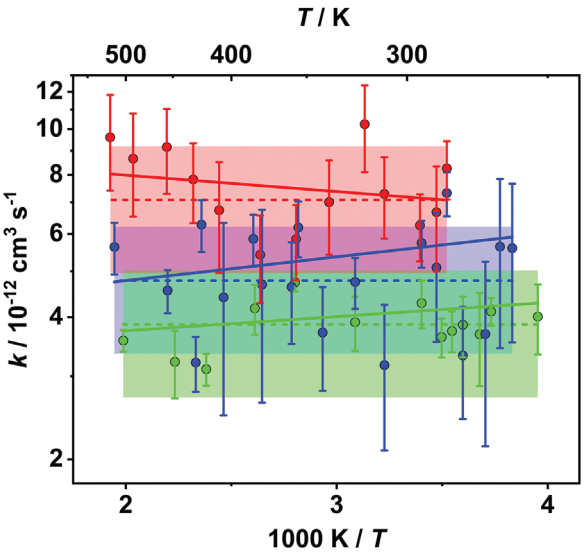

FIGURE 4 | Arrhenius plots for the reactions of OH with (green) OME-1, (blue) OME-2, and (red) OME-3; (symbols) experimental values $\langle k \rangle \pm \sigma_{\langle k \rangle}$ from Table 1 with (solid lines) least-squares fits, (dashed lines) averaged rate coefficients $\langle k \rangle_T$ according to Table 2, and (shaded areas) estimated uncertainty margins of ±30% for $\langle k \rangle_T$.

$[OME\text{-}2]_0$ variations (i.e., no hysteresis in the pseudo-first order plots). We quantify the uncertainty of the data by the root mean square deviation of the $\ln(k_i)$ values with respect to the linearized Arrhenius least-squares fit and obtain for OME-2 + OH a value of $s = 0.253$ (cf. Table 2).

The least-squares fit to the experimental data (obtained with the subroutine FIT from Ref. [27]) is also shown in Figure 4, and the corresponding Arrhenius parameters with their uncertainties ($\pm 2\sigma$) are given in Table 2. Due to the scatter of the data, the slightly negative temperature dependence of $k_{OME\text{-}2+OH}$ formally obtained from the fit is not substantial; the energy of activation does not differ significantly from zero on a 2σ level. We therefore also provide in Table 2 and Figure 4 the temperature-independent mean value $\langle k_{OME2+OH} \rangle_T = (4.78 \pm 0.54) \times 10^{-12}$ cm^3/s obtained as a $(1/\sigma_i^2)$-weighted average of the $\langle k_{OME\text{-}2+OH} \rangle_i$ values given in Table 1.

We note that the *statistical* errors of the rate coefficients are comparatively small, mostly well below 15%. However, we will generally assign an estimated maximum uncertainty of ±30% to also account for possible systematic errors, which may be caused by several influencing factors that are probably minor but are difficult to quantify such as varying flow rates at different temperatures and pressures, possible adsorption effects, side reactions, fluence fluctuations of the photolysis laser, and so on. A value of ±30% has proven reasonable also in comparable earlier, partly collaborative works with other laboratories [24, 26, 28]. A comparison and discussion of the total uncertainties and the significance of the kinetic parameters for the different reactants will be provided below.

3.2 | The Reaction OME-3 + OH

The reaction OME-3 + OH → products was studied in the temperature range 284–519 K at pressures between 0.2 and 10 bar. The approach was the same as for OME-2 + OH. The results are collected in Table 1 and displayed in Figure 4; the primary data are listed in Table S3. No significant pressure dependence of the rate coefficients was observed. From Figure 4, it is obvious that the scatter, though somewhat less than for OME-2 + OH, is still too large to discern a significant temperature dependence (for the formal Arrhenius parameters see Table 2). The average rate coefficient, $\langle k_{OME\text{-}3+OH} \rangle_T$, amounts to $(7.08 \pm 0.88) \times 10^{-12}$ cm^3/s, which is about 50% higher than the value for OME-2 + OH.

3.3 | The Reaction OME-1 + OH

The reaction OME-1 + OH → products was studied in the temperature range 253–503 K at pressures of 0.2, 0.3, 0.6, and 0.9 bar. These experiments supplement recent investigations from this laboratory [9] performed at higher pressures of 2, 5, and 10 bar. The results of the present work are listed in Table 1 and displayed in Figure 4. The primary data are given in Table S1. As in Ref. [9], also at the lower pressures of the present work, no significant pressure dependence was observed.

3.4 | The Reaction TRI + OH

The reaction TRI + OH → products was studied in the temperature range 253–554 K at pressures from 0.2 to 0.9 bar. The results are listed in Table 3 and displayed in Figure 5. The primary data are given in Table S4. Again, no pressure dependence of the rate coefficients could be discerned.

3.5 | The Reactions THF + OH and THF-d8 + OH

The reaction THF (THF-d8) + OH → products were studied in the temperature range 296–495 (297–493) K at pressures from

TABLE 2 | Temperature ranges, pressure ranges, and rate parameters of the R + OH reactions studied in the present work; $k(T) = A \exp[-E_A/(RT)]$ with gas constant R; N is the number of lumped rate coefficients k_i (cf. Tables 1 and 3), s is the estimated root mean square deviation of the $\ln(k_i)$ values from the linearized Arrhenius fit (see footnote[a]), $\langle k \rangle_T$ is the $(1/\sigma_i^2)$-weighted mean of the $\langle k \rangle_i(T)$ values (see text); all error margins in this table represent two standard deviations.

R	T/K	p/bar	$A/10^{-12}$ cm^3/s	(E_A/R)/K	N	s[a]	$\langle k \rangle_T/10^{-12}$ cm^3/s
OME-1	253–503	0.2–0.9	3.26 ± 0.72	−69.1 ± 76.2	13	0.111	3.86 ± 0.24
OME-2	261–514	0.2–5	3.79 ± 1.46	−116.0 ± 135.0	19	0.253	4.78 ± 0.54
OME-3	284–519	0.2–10	9.38 ± 5.66	80.0 ± 206.2	13	0.195	7.08 ± 0.88
TRI	253–554	0.2–0.9	2.22 ± 0.46	−229 ± 80	16	0.079	3.87 ± 0.32
THF	296–495	0.2–0.8	13.1 ± 3.0	−28.4 ± 82.4	10	0.059	14.11 ± 0.51
THF-d8	297–493	0.2–0.8	10.4 ± 1.4	107 ± 50	10	0.070	7.90 ± 0.36

[a] $s = [\chi^2/(N-2)]^{1/2}$ with $\chi^2 = \sum_{i=1}^{N} [\ln k_i - \ln A + E_A/(RT_i)]^2$.

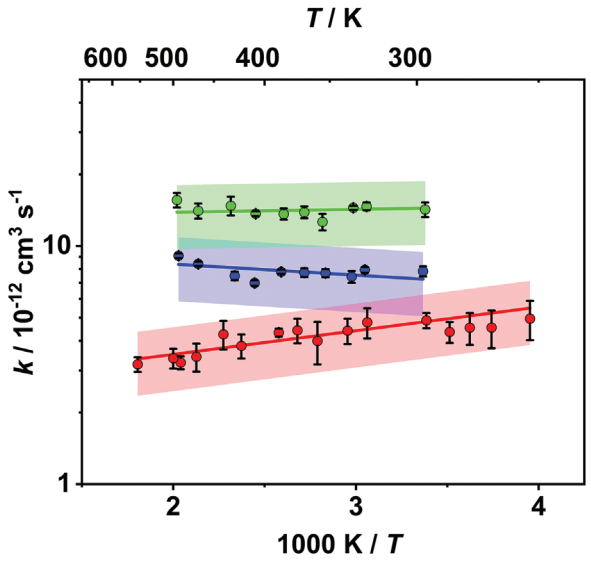

FIGURE 5 | Arrhenius plots for the reactions of OH with (green) THF, (blue) THF-d8, and (red) TRI; (symbols) experimental values $\langle k \rangle \pm \sigma_{\langle k \rangle}$ from Table 3 with (solid lines) least-squares fits (for parameters see Table 2) and (shaded areas) estimated uncertainty margins of ±30% (see text).

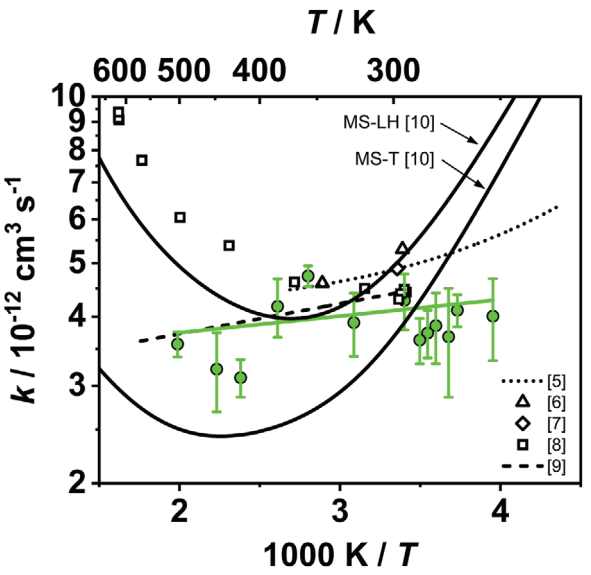

FIGURE 6 | Arrhenius plots for the reaction OME-1 + OH with (green symbols) experimental values $\langle k \rangle \pm \sigma_{\langle k \rangle}$ from Table 1 and (green solid line) the associated least-squares fit (for the parameters see Table 2); the literature data are elucidated in the text.

0.2 to 0.8 bar. The results are listed in Table 3 and displayed in Figure 5. The primary data are given in Table S5 (S6). It becomes obvious that the temperature dependences in the investigated temperature range, while generally very weak, are positive for THF-d8, negative for TRI, and not significant for THF. No notable influence of pressure was observed.

4 | Discussion

4.1 | The Reactions of OH With OME-n (n = 1, 2, 3)

The results from the present work for OH + OME-1 are plotted along with results from other works in Figure 6. Note that for clarity, instead of individual experimental data points from the literature, merely fitted curves are displayed when these were provided in the original publications. It is obvious from Figure 6 that the absolute values of the rate coefficients from all studies are in reasonable agreement whereas the temperature dependences, though generally weak, differ in part. While the majority of the experimental values [5–7, 9] indicate a slightly negative temperature dependence in the range 230 K < T < 570 K, a positive temperature dependence between 293 and 617 K was obtained by Vovelle et al. [8] This difference was already discussed in Ref. [9]. It was noted there that the experiments by Vovelle et al. [8] were essentially conducted at a pressure of 133 mbar whereas the experimental values from Ref. [9] were determined at much higher nominal pressures of 2, 5, and 10 bar. To approach conditions similar to those applied by Vovelle et al. [8], the experiments of the present work were performed at lower pressures from 200 to 900 mbar. But a negative temperature dependence in line with that of Ref. [9] was again obtained, and the positive temperature dependence found in Ref. [8] could not be confirmed.

TABLE 3 | Lumped and averaged (see text) rate coefficients of the reactions of OH with TRI, THF, and THF-d8.

R + OH	$(T \pm \Delta T)$/K	$(\langle k \rangle \pm \sigma_{\langle k \rangle})/10^{-12}$ cm^3/s
TRI + OH	253 ± 7	4.96 ± 0.93
	267 ± 4	4.55 ± 0.82
	276 ± 4	4.54 ± 0.69
	285 ± 2	4.36 ± 0.44
	295 ± 1	4.87 ± 0.36
	327 ± 2	4.78 ± 0.69
	339 ± 2	4.41 ± 0.54
	359 ± 1	4.00 ± 0.81
	373 ± 1	4.43 ± 0.52
	388 ± 1	4.33 ± 0.17
	422 ± 1	3.81 ± 0.44
	440 ± 1	4.26 ± 0.59
	470 ± 1	3.43 ± 0.46
	490 ± 1	3.24 ± 0.20
	500 ± 1	3.38 ± 0.32
	554 ± 1	3.19 ± 0.22
THF + OH	296 ± 1	14.2 ± 1.00
	327 ± 1	14.7 ± 0.56
	335 ± 1	14.5 ± 0.29
	355 ± 1	12.6 ± 0.99
	368 ± 2	13.9 ± 0.78
	384 ± 2	13.6 ± 0.74
	408 ± 1	13.7 ± 0.33
	432 ± 2	14.8 ± 1.33
	468 ± 2	14.1 ± 1.02
	495 ± 1	15.6 ± 1.09
THF-d8 + OH	297 ± 1	7.83 ± 0.38
	328 ± 1	7.94 ± 0.22
	336 ± 1	7.43 ± 0.43
	353 ± 2	7.69 ± 0.30
	368 ± 2	7.73 ± 0.33
	386 ± 1	7.79 ± 0.16
	409 ± 1	6.99 ± 0.19
	428 ± 1	7.49 ± 0.31
	468 ± 1	8.42 ± 0.19
	493 ± 1	9.10 ± 0.22

Also plotted in Figure 6 are two calculated curves from Ref. [10], where slightly different statistical rate theory approaches were used to predict $k_{\text{OME-1+OH}}(T)$. In general, these data were obtained from canonical transition state theory (TST) by assuming an equilibrium between the bimolecular reactants, OME-1 and OH, and a prereactive complex that decomposes in two rate-limiting steps toward the product pairs $H_3COCHOCH_3 + H_2O$ and $H_3COCH_2OCH_2 + H_2O$. The molecular and transition state geometries for the different conformers were optimized with density functional theory (DFT) up to M06-2X/def2-TZVPP, and the barrier heights were calculated at CCSD(T)-F12a/aug-cc-pVTZ level of theory. To account for the effects of multiple conformers, two different approaches were used, a multistructural local harmonic (MS-LH) approximation and a multistructural method for torsional anharmonicity (MS-T) [10, 29, 30].

For comparison, Ref. [10] also reports a calculation within the rigid rotor/harmonic oscillator (RRHO) approximation, including hindered rotor corrections; however, the agreement with the experimental data is significantly worse. Accordingly, these results are not included in Figure 6. Regarding the other two methods, the authors of Ref. [10] emphasize that MS-T can be expected to perform better than MS-LH. They note, however, the larger deviation of the MS-T results from the experimental rate coefficients of Vovelle et al. [8]. As can be seen from Figure 6, the MS-T results are more in line with the negative temperature dependence observed in both Ref. [9] and the present work. Unfortunately, we were unable to extend the temperature range of the present work significantly above 500 K to experimentally confirm and/or localize more precisely the position of the predicted minimum in the Arrhenius plot. Such shallow minima are not uncommon for this type of reaction proceeding via prereactive complexes (see, e.g., [31]).

In Figure 7, the rate coefficients for OME-2 + OH and OME-3 + OH experimentally determined in the present work are compared with calculated and estimated values from the literature. As was already mentioned in the introduction section, there appear to be no other experimental kinetic data on these reactions published so far. Based on theoretical rate coefficients for the OME-1 + OH reaction, which mainly involves H abstractions, He et al. [10] estimated rate coefficients for the reactions of OH with the higher homologs OME-2 and OME-3 by multiplying the temperature-independent *A*-factors of the extended Arrhenius expressions for H abstraction from CH_2 by the number of CH_2 groups (see Supplementary data of Ref. [10]). The contributions from the two CH_3 groups were kept unaltered. The results are plotted in Figure 7. Also plotted are estimated values from Dinelli et al. [12], which were obtained by a reaction class/lumping approach based on the rate coefficients for H abstraction from OME-1 [32]. Both estimations show for OME-2 as well as for OME-3 a very good agreement with the experimental data of the present work. For both reactants, they predict a very weak temperature dependence of the rate coefficients over the studied temperature range with somewhat higher absolute values for OME-3 + OH than for OME-2 + OH (approximately a factor of 1.3 at 300 K), which is in line with the experimental findings of the present work.

For OME-3, another calculated curve, from Zhu et al. [11], is shown in Figure 7. These results were obtained from transition state theory with molecular data from DFT at M062X/6-311++G(d,p) level of theory and single-point energies from complete basis set extrapolations of QCISD(T) results (for details see Ref. [11]). The agreement of these calculated values with the experimental results of the present work is slightly worse compared to the estimations from He et al. [10] The calculations in particular seem to underestimate the rate coefficients for temperatures above ca. 300 K and also predict a too

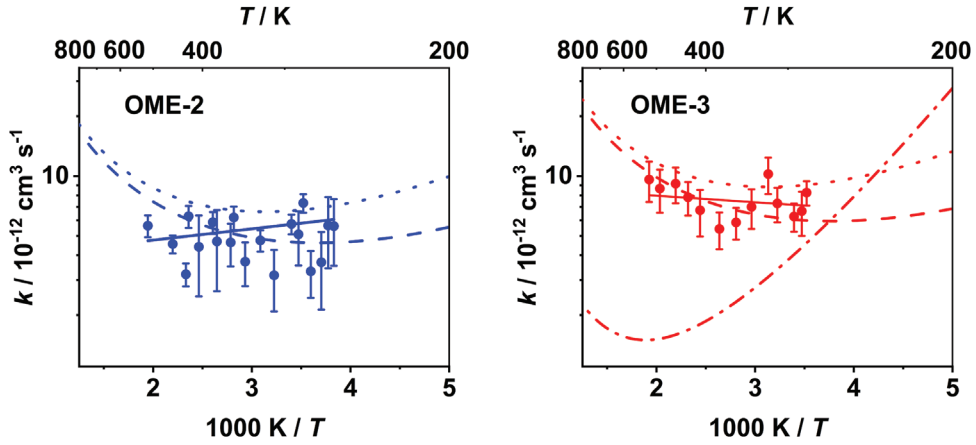

FIGURE 7 | Arrhenius plots for the reactions of OH with (blue) OME-2 and (red) OME-3; (symbols) experimental values $\langle k \rangle \pm \sigma_{\langle k \rangle}$ from Table 1, (solid lines) least-squares fits (for parameters see Table 2), estimations from (dashed lines) He et al. [10] and (dotted lines) Dinelli et al. [12], calculations from (dash-dotted line) Zhu et al. [11].

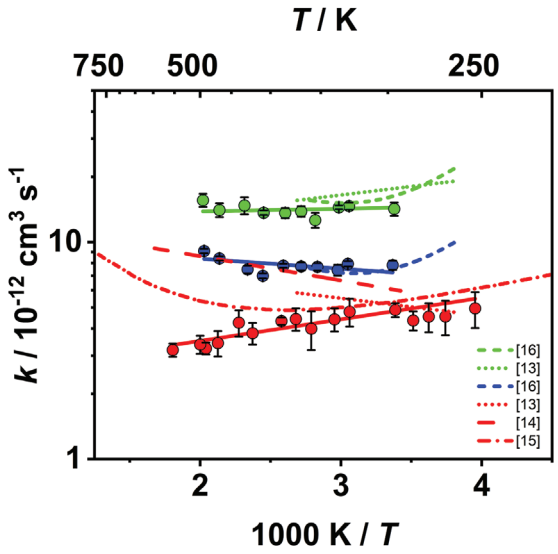

FIGURE 8 | Arrhenius plots for the reactions of OH with (green) THF, (blue) THF-d8, and (red) TRI; (symbols) experimental values $\langle k \rangle \pm \sigma_{\langle k \rangle}$ from Table 3 with (solid lines) least-squares fits (for parameters see Table 2); the literature data are elucidated in the text.

strong negative temperature dependence in the range below 500 K.

4.2 | The Reactions of OH With THF, THF-d8, and TRI

The experimentally determined rate coefficients for the reactions of OH with the three cyclic ethers are displayed and compared with literature data in Figure 8. Again, for the sake of clarity, no single experimental data points for the literature values are plotted but only fits as given in the original works are shown [13, 14, 16]. In general, the absolute values of the rate coefficients are on the same order of magnitude than those for OME-n + OH with $k_{\mathrm{THF+OH}}$ being a factor of 3 to 4 larger than $k_{\mathrm{TRI+OH}}$, and the latter value lying closer to $k_{\mathrm{OME\text{-}}n\mathrm{+OH}}$. A normal primary isotope effect is observed between THF and THF-d8 with $k_{\mathrm{THF+OH}}/k_{\mathrm{THF\text{-}d8+OH}} \sim 2$. The temperature dependences for all three reactions are, in general, very weak, with a small negative temperature dependence discernible for the TRI + OH experimental values from the present work.

Figure 8 shows that the experimental data for THF and THF-d8 from the present study are in very good agreement with the literature values. The experiments by both Illés et al. [16] and Moriarty et al. [13] indicate a weakly negative temperature dependence at $T < 300$ K, which turns through a shallow minimum near 300 K into a slightly positive temperature dependence at higher temperatures. This general trend is confirmed by the data of the present work for temperatures up to 500 K.

The situation for TRI + OH is somewhat less satisfactory. The absolute values of the rate coefficients from all three experimental studies are again in very good agreement for temperatures below ca. 300 K. But while the works of Moriarty et al. [13] and Zabarnick et al. [14] report a slight positive temperature dependence, a slight negative temperature dependence is obtained in the present work. This different behavior leads to a factor of three discrepancy in the rate coefficients at temperatures near 500 K (cf. Figure 8).

A curve calculated by Saheb and Bahadori [15] for the TRI + OH reaction is also shown in Figure 8. These authors performed canonical variational transition state theory calculations with a two-transition-state model, using the VariFlex code [33]. The necessary molecular and transition state data were obtained from quantum chemical calculations at several different levels of theory (M05-2X, M06-2X, MPWB1K, and CBS-QB3) [15]. Unfortunately, there is some inconsistency in the numerical and graphical presentation of the results in Ref. [15]. For Figure 8, we adopted the CBS-QB3-based curve digitized from Figure 6 of Ref. [15]. The CBS-QB3 results were chosen because they represent the highest level of theory applied there. It becomes obvious that the calculations predict a U-shaped Arrhenius curve (as also do all the other methods applied in Ref. [15]) with a shallow minimum near 400 K. The calculated curve, while being in very good agreement with the absolute values of the measured rate coefficients, does not allow, however, to resolve the discrepancy between the different temperature dependences found in the experiments.

4.3 | Structural Effects

By now, it is well accepted that the molecular mechanism of OH + ether reactions is H abstraction from CH_n to form H_2O and the complementary carbon-centered radical. The rate coefficients of these reactions are usually larger than those of the corresponding OH + alkane reactions [34]. The increased reactivity is attributed to the presence of oxygen atoms in the carbon backbone, which lowers the C–H bond dissociation energies (BDE) by 20–25 kJ/mol (see, e.g., [35]) and enables the formation of hydrogen-bonded prereactive complexes [5, 13, 34, 36, 37]. This activation effect is more pronounced in diethers than in monoethers and does not seem to be confined to CH_n groups in α-position to the oxygen atoms but extends to β- and γ-positions and possibly beyond [34]. In general, branching ratios between abstractions from different CH_n groups are not readily accessible in conventional kinetic experiments, where usually overall rate coefficients are determined. Typically, results from theoretical calculations must be additionally employed (see, e.g., [38]). Nonetheless, from suitable combinations of overall rate coefficients for different OH + ether reactions, site-specific group rate coefficients have been estimated [34]. It turned out that for unbranched alkyl ethers, H abstraction from α-CH_n via a five-membered ring transition state seems to predominate, and contributions from other CH_n groups decrease with increasing separation from the O atom [34]. This predominance was confirmed by theoretical calculations in Ref. [38] (for higher temperatures between 900 and 1300 K).

In the following, we compare the experimental results of the present work with data available in the literature and discuss possible structural influences on the ether + OH kinetics. Since, under the conditions of this study, the rate coefficients of the investigated reactions show only little temperature dependence, we initially neglect the dependence on temperature and use the average values $\langle k \rangle_T$ from Table 2 as a convenient measure for comparison.

For THF, the only cyclic monoether of this study, $\langle k \rangle_T = (14.11 \pm 0.51) \times 10^{-12}$ cm^3/s in the temperature range 296–495 K. For diethyl ether (DEE), which may be considered as an open-chain analog of THF, rate coefficients of its reaction with OH between 16.8×10^{-12} cm^3/s at 240 K and 11.6×10^{-12} cm^3/s at 442 K were recommended in an earlier review [39] on the basis of several experimental studies. It is obvious that the $\langle k \rangle_T$ value of THF is within this range. Also the measured isotope effects, k(OH+THF)/k(OH+THF-d8) ranging from 1.99 to 1.66 for T = 297 to 493 K (cf. Table 2) and k(OH+DEE)/k(OH+DEE-d10) ranging from 2.0 to 1.7 for T = 296 to 441 K [40] virtually agree with each other. Obviously, the reactivity of OH toward THF and DEE is very similar in the studied temperature range. The reduced reactivity toward cyclic ethers relative to their open-chain analogs discussed in Refs. [13, 34] is, at least for this reactant pair, not discernible within the given uncertainty ranges. We also note that calculated bond dissociation energies in THF and DEE, in particular for the α-CH_2 groups, are close to each other: BDE(THF, α-CH_2) = 389.6 kJ/mol, BDE(THF, β-CH_2) = 408.4 kJ/mol (CCSD(T) and W1U calculations, isodesmic reactions) [16]; BDE(DEE, CH_2) = 392.5 kJ/mol and BDE(DEE, CH_3) = 423.3 kJ/mol (G4 calculations) [41]. Despite the different quantum chemical methods used, the similarity of the calculated BDEs for THF and DEE supports the similarity of the rate coefficients for OH + THF and OH + DEE. Furthermore, in both ethers, H abstraction from α-position is possibly preferred over abstraction from β-position. It is well known (see, e.g., [42]) that for a series of abstraction reactions by a particular attacking radical, often a rough correlation exists between the energies of activation (and hence, to a first approximation, the rate coefficients) and the bond dissociation energies of the breaking bonds.

The situation for the oligoethers OME-1, OME-2, OME-3, and TRI is different from the situation of the higher monoethers insofar as only α-CH_n groups occur in these species. In going from OME-1 to OME-3, the number of CH_3 groups remains constant (two), and the number of CH_2 groups increases from one to three. Inspection of Table 2 reveals a respective increase of $\langle k \rangle_T/10^{-12}$ cm^3/s from ~3.9 via ~4.8 to ~7.1 in line with the number of CH_n groups. The cyclic ether TRI, containing solely three CH_2 groups, has a value of $\langle k \rangle_T \sim 3.9 \times 10^{-12}$ cm^3/s in virtual agreement with the value for OME-1. Both ethers contain three CH_n groups, which obviously exhibit a very similar reactivity toward OH. It seems as if in OMEs the reactivity of the internal CH_2 and the terminal CH_3 groups toward OH do not strongly differ if corrected for statistical effects. This finding is again supported by very similar C–H bond dissociation energies. Zhu et al. [11] performed combined CBS-APNO/G3/G4 calculations for the entire series OME-1 to OME-5 and obtained values in the range 397.6–400.1 kJ/mol for CH_3 and 397.1–404.9 kJ/mol for CH_2 with the terminal CH_3 groups almost consistently exhibiting somewhat lower values than the secondary CH_2 groups, a result also obtained in Ref. [43].

In general, the investigations of the present work confirm for OME-1, TRI, and THF/THF-d8 earlier experimental results and the qualitative structure-reactivity discussions presented in Refs. [13, 34]. The rate coefficients are larger than those of the corresponding OH + alkane reactions but (except for THF) distinctly lower than predicted by common structure-reactivity relationships [44], a known discrepancy in particular for polyethers [45]. For OME-1 and TRI, which contain identical numbers of α-CH_n groups, the rate coefficients are very similar, indicating that α-CH_3 and α-CH_2 groups have comparable reactivities toward OH (see also [13]). There is, at least for these two compounds, no significant difference between the reactivities of the ring and the open-chain structure, in contrast to what is observed for ethers containing –$(CH_2)_n$– moieties with $n \geq 2$. In the latter cases, the open-chain isomers are commonly more reactive [13, 34]. The reactions of OH with the higher open-chain homologs OME-2 and OME-3, which were experimentally studied for the first time in this work, fit nicely into this picture. The rate coefficients at 298 K (Arrhenius parameters from Table 2) increase for OME-1 → OME-2 → OME-3 by increments of ~1.5×10^{-12} cm^3/s per CH_2 group. All rate coefficients determined in this work show no discernible pressure dependence and at most a very weak temperature dependence.

5 | Summary

Rate coefficients of the reactions of OH radicals with OME-2 (T = 261–514 K, p = 0.2–5.0 bar, He) and OME-3 (T = 284–519 K,

p = 0.2–10 bar, He) were experimentally determined for the first time. No significant temperature and pressure dependences were observed. The rate coefficients averaged over the experimental temperature ranges are $\langle k \rangle_T(\mathrm{OH} + \mathrm{OME\text{-}2}) = (4.78 \pm 0.54) \times 10^{-12}$ $\mathrm{cm^3/s}$ and $\langle k \rangle_T(\mathrm{OH} + \mathrm{OME\text{-}3}) = (7.08 \pm 0.88) \times 10^{-12}$ $\mathrm{cm^3/s}$.

Analogous experiments were performed for the reactions of OH radicals with OME-1, TRI, THF, and THF-d8. Rate coefficients in good agreement with values in the literature were obtained. The detailed results of all studied reactions are collected in Table 2.

The measured rate coefficients were examined in terms of structure-reactivity relationships. In earlier works [13, 34, 45], it was found that simple estimations based on group contributions usually overpredict the reactivity of CH_n groups in oligoethers toward OH. In the present work, it was shown that this is also true for OH + OME-2 and OH + OME-3.

Detailed quantum chemical and statistical rate theory calculations would be necessary to gain further mechanistic insight into these complex-forming bimolecular reactions. However, the differences between the experimental rate coefficients obtained in the present work are small, their temperature and pressure dependences are weak. In view of the subtle effects to be expected from close-lying molecular and transition state energies and from multiple conformations of the oligoether backbones, rather high levels of theory are required. Furthermore, the significance of such calculations would be greatly enhanced by a comparison with experimental results obtained over a wider temperature range, where the temperature dependence may be more pronounced. Such investigations, which would require alternative experimental approaches, for example, shock tube studies, are beyond the scope of the present work. Accordingly, the extensive calculations necessary for an adequate description of the studied OH + oligoether reactions over reasonable ranges of temperature and pressure should also be reserved for future investigations.

Acknowledgments

Funded by the Deutsche Forschungsgemeinschaft (DFG, German Research Foundation)–Projektnummer 237267381–TRR 150. The authors thank Clara Strunz for help with some of the experiments.

Open access funding enabled and organized by Projekt DEAL.

Data Availability Statement

The data that support the findings of this study are available from the corresponding author upon reasonable request.

References

1. J. Burger, M. Siegert, E. Ströver, and H. Hasse, "Poly(oxymethylene) Dimethyl Ethers as Components of Tailored Diesel Fuel: Properties, Synthesis and Purifications Concepts," *Fuel* 89 (2010): 3315–3319, https://doi.org/10.1016/j.fuel.2010.05.014.

2. H. Liu, Z. Wang, J. Wang, et al., "Performance, Combustion and Emission Characteristics of a Diesel Engine Fueled With Polyoxymethylene Dimethyl Ethers ($PODE_{3-4}$)/Diesel Blends," *Energy* 88 (2015): 793–800, https://doi.org/10.1016/j.energy.2015.05.088.

3. H. Pitsch, D. Goeb, L. Cai, and W. Willems, "Potential of Oxymethylene Ethers as Renewable Diesel Substitute," *Progress in Energy and Combustion Science* 104 (2024): 101173, https://doi.org/10.1016/j.pecs.2024.101173.

4. Y. Fenard and G. Vanhove, "A Mini-Review on the Advances in Kinetic Understanding of the Combustion of Linear and Cyclic Oxymethylene Ethers," *Energy & Fuels* 35 (2021): 14325–14342, https://doi.org/10.1021/acs.energyfuels.1c01924.

5. E. Porter, J. Wenger, J. Treacy, et al., "Kinetic Studies on the Reaction of Hydroxyl Radicals With Diethers and Hydroxyethers," *Journal of Physical Chemistry A* 101 (1997): 5770–5775, https://doi.org/10.1021/jp971254i.

6. T. J. Wallington, M. D. Hurley, J. C. Ball, et al., "Atmospheric Chemistry of Dimethoxymethane ($CH_3OCH_2OCH_3$): Kinetics and Mechanism of Its Reaction With OH Radicals and Fate of the Alkoxy Radicals $CH_3OCHO(\bullet)OCH_3$ and $CH_3OCH_2OCH_2O(\bullet)$," *Journal of Physical Chemistry A* 101 (1997): 5302–5308, https://doi.org/10.1021/jp9631184.

7. L. P. Thüner, I. Barnes, T. Maurer, C. G. Sauer, and K. H. Becker, "Kinetic Study of the Reaction of OH With a Series of Acetals at 298 ± 4 K," *International Journal of Chemical Kinetics* 31 (1999): 797–803, https://doi.org/10.1002/(SICI)1097-4601(1999)31:11%3C797::AID-JCK6%3E3.0.CO;2-C.

8. C. Vovelle, A. Bonard, V. Daele, and J.-L. Delfau, "Kinetics of OH Radical Reactions With a Series of Symmetric Acetals in the Temperature Range 293–617 K," *Physical Chemistry Chemical Physics* 3 (2001): 4939–4945, https://doi.org/10.1039/b105650f.

9. C. Bänsch and M. Olzmann, "Reaction of Dimethoxymethane With Hydroxyl Radicals: An Experimental Kinetic Study at Temperatures Above 296 K and Pressures of 2, 5, and 10 Bar," *Chemical Physics Letters* 720 (2019): 19–24, https://doi.org/10.1016/j.cplett.2019.01.053.

10. T. He, Z. Wang, X. You, et al., "A Chemical Kinetic Mechanism for the Low- and Intermediate-Temperature Combustion of Polyoxymethylene Dimethyl Ether 3 ($PODE_3$)," *Fuel* 212 (2018): 223–235, https://doi.org/10.1016/j.fuel.2017.09.080.

11. Q. Zhu, J.-Y. Lyu, R. He, X. Bai, Y. Li, and W. Yang, "Detailed Kinetic Mechanism of Polyoxymethylene Dimethyl Ether 3 (PODE3). Part I: Ab Initio Thermochemistry and Kinetic Predictions for Key Reactions," *Combustion and Flame* 256 (2023): 112990, https://doi.org/10.1016/j.combustflame.2023.112990.

12. T. Dinelli, A. Pegurri, A. Bertolino, et al., "A Data-Driven, Lumped Kinetic Modeling of OME_{2-5} Pyrolysis and Oxidation," *Proceedings of the Combustion Institute* 40 (2024): 105547, https://doi.org/10.1016/j.proci.2024.105547.

13. J. Moriarty, H. Sidebottom, J. Wenger, A. Mellouki, and G. Le Bras, "Kinetic Studies on the Reactions of Hydroxyl Radicals With Cyclic Ethers and Aliphatic Diethers," *Journal of Physical Chemistry A* 107 (2003): 1499–1505, https://doi.org/10.1021/jp021267i.

14. S. Zabarnick, J. W. Fleming, and L. MC, "Kinetics of Hydroxyl Radical Reactions With Formaldehyde and 1,3,5-Trioxane Between 290 and 600 K," *International Journal of Chemical Kinetics* 20 (1988): 117–129, https://doi.org/10.1002/kin.550200205S.

15. V. Saheb and A. Bahadori, "Theoretical Studies on the Kinetics of the Hydrogen-Abstraction Reactions From 1,3,5-Trioxane and 1,4-Dioxane by OH Radicals," *Progress in Reaction Kinetics and Mechanism* 45 (2020): 1–13, https://doi.org/10.1177/1468678319899252.

16. Á. Illés, Z. B. Rózsa, R. Thangaraj, et al., "An Experimental and Theoretical Kinetic Study of the Reactions of Hydroxyl Radicals With Tetrahydrofuran and Two Deuterated Tetrahydrofurans," *Chemical Physics Letters* 776 (2021): 138698, https://doi.org/10.1016/j.cplett.2021.138698.

17. B. R. Giri, F. Khaled, M. Szőri, B. Viskolcz, and A. Farooq, "An Experimental and Theoretical Kinetic Study of the Reaction of OH Radicals With Tetrahydrofuran," *Proceedings of the Combustion Institute* 36 (2017): 143–150, https://doi.org/10.1016/j.proci.2016.06.016.

18. L.-S. Tran, O. Herbinet, H.-H. Carstensen, and F. Battin-Leclerc, "Chemical Kinetics of Cyclic Ethers in Combustion," *Progress in Energy and Combustion Science* 92 (2022): 101019, https://doi.org/10.1016/j.pecs.2022.101019.

19. R. Forster, M. Frost, D. Fulle, et al., "High Pressure Range of the Addition of HO to HO, NO, NO_2, and CO. I. Saturated Laser Induced Fluorescence Measurements at 298 K," *Journal of Chemical Physics* 103 (1995): 2949–2958, https://doi.org/10.1063/1.470482.

20. H. Hippler, F. Striebel, and B. Viskolcz, "A Detailed Experimental and Theoretical Study on the Decomposition of Methoxy Radicals," *Physical Chemistry Chemical Physics* 3 (2001): 2450–2458, https://doi.org/10.1039/B101376I.

21. O. Welz, F. Striebel, and M. Olzmann, "On the Thermal Unimolecular Decomposition of the Cyclohexoxy Radical—An Experimental and Theoretical Study," *Physical Chemistry Chemical Physics* 10 (2008): 320–329, https://doi.org/10.1039/B713286G.

22. O. Welz and M. Olzmann, "Kinetics of the NCN + No Reaction Over a Broad Temperature and Pressure Range," *Journal of Physical Chemistry A* 116 (2012): 7293–7301, https://doi.org/10.1021/jp303069g.

23. C. A. Whelan, J. Eble, Z. S. Mir, et al., "Kinetics of the Reactions of Hydroxyl Radicals With Furan and Its Alkylated Derivatives 2-Methyl Furan and 2,5-Dimethyl Furan," *Journal of Physical Chemistry A* 124 (2020): 7416–7426, https://doi.org/10.1021/acs.jpca.0c06321.

24. N. C. K. Robertson, L. Onel, M. A. Blitz, et al., "Temperature-Dependent, Site-Specific Rate Coefficients for the Reaction of OH (OD) With Methyl Formate Isotopologues via Experimental and Theoretical Studies," *Journal of Physical Chemistry A* 128 (2024): 5028–5040, https://doi.org/10.1021/acs.jpca.4c02524.

25. L. Lautenschütz, D. Oestreich, P. Haltenort, U. Arnold, E. Dinjus, and J. Sauer, "Efficient Synthesis of Oxymethylene Dimethyl Ethers (OME) From Dimethoxymethane and Trioxane over Zeolites," *Fuel Processing Technology* 165 (2017): 27–33, https://doi.org/10.1016/j.fuproc.2017.05.005.

26. C. Bänsch, J. Kiecherer, M. Szőri, and M. Olzmann, "Reaction of Dimethylether With Hydroxyl Radicals: Kinetic Isotope Effect and Prereactive Complex Formation," *Journal of Physical Chemistry A* 117 (2013): 8343–8351, https://doi.org/10.1021/jp405724a.

27. W. H. Press, B. P. Flannery, S. A. Teukolsky, and W. T. Vetterling, *Numerical Recipes (FORTRAN Version)* (Cambridge University Press, 1989).

28. C. Kappler, J. Zádor, O. Welz, R. X. Fernandes, M. Olzmann, and C. A. Taatjes, "Competing Channels in the Propene + OH Reaction: Experiment and Validated Modeling Over a Broad Temperature and Pressure Range," *Zeitschrift Fur Physikalische Chemie* 225 (2011): 1271–1291, https://doi.org/10.1524/zpch.2011.0165.

29. T. Yu, J. Zheng, and D. G. Truhlar, "Multi-Structural Variational Transition State Theory. Kinetics of the 1,4-Hydrogen Shift Isomerization of the Pentyl Radical With Torsional Anharmonicity," *Chemical Science* 2 (2011): 2199–2213, https://doi.org/10.1039/c1sc00225b.

30. J. Zheng, S. L. Mielke, K. Clarkson, and D. G. Truhlar, "MSTor: A Program for Calculating Partition Functions, Free Energies, Enthalpies, Entropies, and Heat Capacities of Complex Molecules Including Torsional Anharmonicity," *Computer Physics Communications* 183 (2012): 1803–1812, https://doi.org/10.1016/j.cpc.2012.03.007.

31. C.-W. Zhou, J. M. Simmie, and H. J. Curran, "An Ab Initio/Rice-Ramsperger-Kassel-Marcus Study of the Hydrogen-Abstraction Reactions of Methyl Ethers, $H_3COCH_{3-x}(CH_3)_x$, X = 0–2, by OH; Mechanism and Kinetics," *Physical Chemistry Chemical Physics* 12 (2010): 7221–7233, https://doi.org/10.1039/c002911d.

32. A. Pegurri, T. Dinelli, L. P. Maffai, T. Faravelli, and A. Stagni, "Coupling Chemical Lumping to Data-Driven Optimization for the Kinetic Modeling of Dimethoxymethane (DMM) Combustion," *Combustion and Flame* 260 (2024): 113202, https://doi.org/10.1016/j.combustflame.2023.113202.

33. S. J. Klippenstein, A. F. Wagner, R. C. Dunbar, D. M. Wardlaw, and S. H. Robertson, VariFlex, Version 1.00 (1999).

34. A. Mellouki, G. Le Bras, and H. Sidebottom, "Kinetics and Mechanisms of the Oxidation of Oxygenated Organic Compounds in the Gas Phase," *Chemical Reviews* 103 (2003): 5077–5096, https://doi.org/10.1021/cr020526x.

35. Y.-R. Luo, *Handbook of Bond Dissociation Energies in Organic Compounds* (CRC Press, 2002), https://doi.org/10.1201/9781420039863.

36. I. W. M. Smith and A. R. Ravishankara, "Role of Hydrogen-Bonded Intermediates in the Bimolecular Reactions of the Hydroxyl Radical," *Journal of Physical Chemistry A* 106 (2002): 4798–4807, https://doi.org/10.1021/jp014234w.

37. C. Zavala-Oseguera, J. R. Alvarez-Idaboy, G. Merino, and A. Galano, "OH Radical Gas Phase Reactions With Aliphatic Ethers: A Variational Transition State Theory Study," *Journal of Physical Chemistry A* 113 (2009): 13913–13920, https://doi.org/10.1021/jp906144d.

38. M. Belmekki, B. R. Giri, D. Liu, and A. Farooq, "Symmetric Ethers as Bioderived Fuels: Reactivity With OH Radicals," *Energy & Fuels* 35 (2021): 16075–16085, https://doi.org/10.1021/acs.energyfuels.1c01408.

39. R. Atkinson, "Gas-Phase Tropospheric Chemistry of Organic Compounds," *Journal of Physical and Chemical Reference Data* (1994). Monograph No. 2.

40. T. J. Wallington, R. Liu, P. Dagaut, and M. J. Kurylo, "The Gas Phase Reactions of Hydroxyl Radicals With a Series of Aliphatic Ethers Over the Temperature Range 240–440 K," *International Journal of Chemical Kinetics* 20 (1988): 41–49, https://doi.org/10.1002/kin.550200106.

41. Y. L. Shang, J. C. Shi, L. M. Fang, Q. G. Feng, H. Y. Wang, and S. N. Luo, "Theoretical Investigation on Hydrogen Abstraction by NO_2 From Symmetric Ethers $(CH_3)_{2x}O$ (x = 1–4)," *Journal of Physical Chemistry A* 122 (2018): 6829–6841, https://doi.org/10.1021/acs.jpca.8b04943.

42. J. A. Kerr, "Metathetical Reactions of Atoms and Radicals," in *Comprehensive Chemical Kinetics, Volume 18: Selected Elementary Reactions*, ed. C. H. Bamford and C. F. H. Tipper (Elsevier, 1976), 39–109.

43. W. Sun, W. Guoqing, L. Shuang, et al., "Speciation and the Laminar Burning Velocities of Poly(oxymethylene) Dimethyl Ether 3 ($POMDME_3$) Flames: An Experimental and Modeling Study," *Proceedings of the Combustion Institute* 36 (2017): 1269–1278, https://doi.org/10.1016/j.proci.2016.05.058.

44. R. Atkinson, "Kinetics and Mechanisms of the Gas-Phase Reactions of the Hydroxyl Radical With Organic Compounds Under Atmospheric Conditions," *Chemical Reviews* 85 (1985): 69–201, https://doi.org/10.1021/cr00071a004.

45. E. S. C. Kwok and R. Atkinson, "Estimation of Hydroxyl Radical Reaction Rate Constants for Gas-Phase Organic Compounds Using a Structure-Reactivity Relationship: An Update," *Atmospheric Environment* 29 (1995): 1685–1695, https://doi.org/10.1016/1352-2310(95)00069-B.

Supporting Information

Additional supporting information can be found online in the Supporting Information section.

Supporting Information